Supplementary material for

Numerical Study of Circulating Tumor Cell Behavior in Constricted Microvessels Based on Immersed Boundary-Lattice Boltzmann Method

Mingzhe Zhang †[a], Jun Shen †[b], Runkeng Liu [a], Peilin Cui [a], Huiying Wu [a], Zhenyu Liu *[a]

a. School of Mechanical Engineering, Shanghai Jiao Tong University, Shanghai, China 200240

b. Zhongshan Hospital Wusong Branch, Fudan University, Shanghai, China 200940

† These authors contributed equally to this paper.

* Corresponding author, Email: zhenyu.liu@sjtu.edu.cn

Details for solid phase modeling

The coarse-grained spectral linking membrane model is used for the solid phase modeling. The model incorporates four main types of forces, each representing a specific mechanical behavior: [S1]

The link force acts along the links and represents the reaction to stretching and compression of the underlying spectrin-network beneath the links.

$$F_{link} = -\frac{k_l dL}{p}\left[1 + \frac{1}{\tau_l^2 - dL^2}\right] \tag{S1}$$

where $dL = \frac{L_i - L_0}{L_0}$ is the normal strain, p is the persistence-length of a spectrin filament that equals 7.5 nm, and $\tau_l = 3.00$ is the relative expansion ratio at which the spectrin-network reaches its persistence length.

The bending force acts between adjacent cell surface elements, reflecting the membrane's reactive response due to the underlying cytoskeleton and the non-zero thickness of the spectrin-network. This force is applied in the normal direction of each surface element.

$$F_{bend} = -\frac{k_b d\theta}{L_0}[1 + \frac{1}{\tau_b^2 - d\theta^2}] \tag{S2}$$

where $d\theta = \theta_i - \theta_0$, and $\tau_b = \frac{\pi}{6}$ is the limiting angle. Using the micropipette aspiration images, τ_b is calibrated for this problem and it is chosen to prevents unrealistic sharp surface edges. [S1]

The local surface conservation force reflects the response of the membrane and the spectrin-network to stretching and compression. It acts on each surface element, evenly distributed across

the three vertices of the cell surface triangles, and directed toward the centroid of these triangle.

$$F_{area} = -\frac{k_a dA}{L_0}[1 + \frac{1}{\tau_a^2 - dA^2}] \quad \text{(S3)}$$

where $dA = \frac{A_i - A_0}{A_0}$ is the relative deviation from the initial area and $\tau_b = 0.30$ is the limiting factor to prohibit surface area changes more than 30%. For dA near 30%, the area force gets large enough to stop further expansion of the surface area. Large changes in the surface area can lead to permanent damages to the cell membrane.

The volume conservation force applies globally to all nodes of the cell, ensuring the cell's quasi-incompressibility. It is directed along the normal of each surface triangle.

$$F_{volume} = -\frac{k_v dV}{L_0}[1 + \frac{1}{\tau_v^2 - dV^2}] \quad \text{(S4)}$$

where $dV = \frac{V_i - V_0}{V_0}$ is the relative deviation from initial volume and $\tau_v = 0.01$ is the limiting factor to resist changes in the cell volume.

The combined effect of these forces enables the model to accurately simulate the dynamic behavior of the cells in the flow. The stiffness of the cells can be modulated by adjusting the three free parameters in the constitutive model: k_l, k_b, k_a and k_v.

The cell stiffness is characterized using the surface Young's modulus parameter (Es), which can be derived from optical tweezer simulations. [S2] In the simulation, a number of vertices on opposite sides of the cell membrane, approximately 2% on each side, are selected to simulate the contact region of the optical tweezers. A constant force is maintained to allow the red blood cell (RBC) to reach equilibrium. By measuring the axial diameter along the stretching direction and the transverse diameter perpendicular to it, strain is computed based on the relationship between force and deformation, and described using to the formula calculate the surface Young's modulus (Es) of the cell.

$$E_s = \sqrt{\frac{1}{125rB}[\frac{F}{\varepsilon}]^3} \quad \text{(S5)}$$

Assuming the initial diameter of the cell is L_0 and the longest diameter after deformation is L, the stretch ratio of the cell is defined as $\varepsilon = \frac{L}{L_0}$. B represents the bending modulus of the cell, r is the initial radius of the cell, and F is the force applied at both ends of the cell.

Geometry and boundary conditions

In this study, the adopt of periodic boundary conditions in the simulation is reasonable and

represents a common approach in current blood flow simulations, although it does not fully reflect the actual conditions in real blood vessels. Relevant literature includes the work by Wang et al. [S3], who simulated a thrombosed vessel with a total length of 45 μm, including a 15 μm stenosed segment. The periodic boundary conditions were applied at both inlet and outlet. Their study showed that at low Reynolds numbers, RBCs influence the blood flow and enhance the deposition of freely flowing platelets onto the thrombus. Similarly, Ye et al. [S4] modeled thrombus formation in a cylindrical vessel with a stenosed region. The total vessel length was 74 μm, with the stenosed segment measuring 18 μm. The periodic boundary conditions were also used at both ends. By studying the circulation of nanoparticles and microparticles (including spherical particles and filamentous nanoworms) in RBC suspensions through the constricted channel mimicking microvascular stenosis, they found that the accumulation of 1 μm diameter spherical particles in the stenosed region increases with both the length and degree of stenosis. This was attributed to the interactions between spheres and RBCs.

To evaluate whether a total vessel length of 50 μm is reasonable in the current study, we increased the total length from 50 μm to 70 μm while keeping the stenosed segment unchanged. All other simulation parameters were held constant. Fig. S1 shows the variation of CTC velocity over time. The curves for vessel lengths of 70 μm and 50 μm are nearly identical, and both show CTC adhesion during the vessel constriction. Therefore, although the use of periodic boundary conditions in the simulation does not fully represent real blood flow conditions, it is nonetheless a reasonable and justified approach.

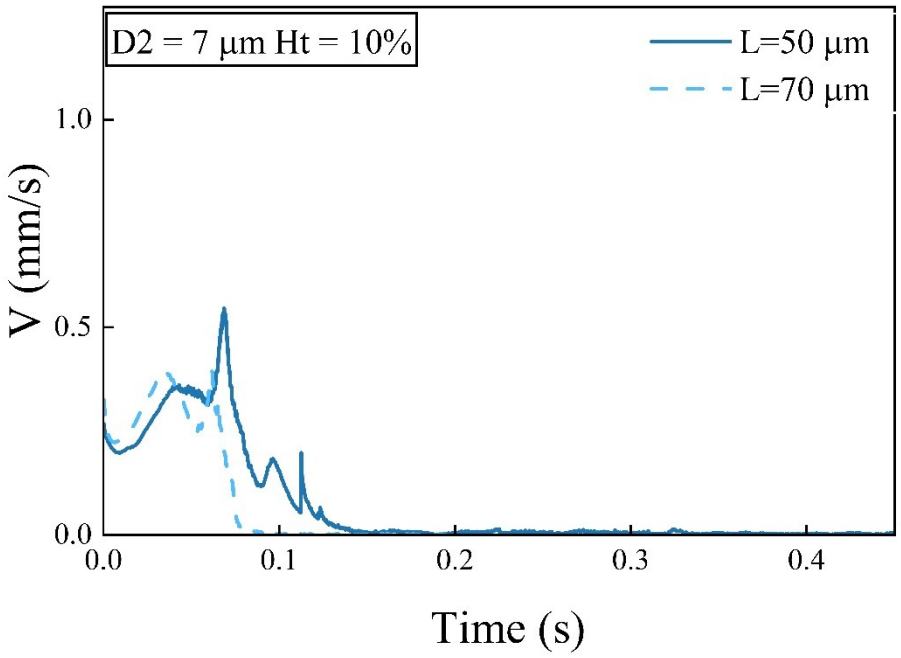

Fig. S1. CTC velocity over time

Mesh and time-step convergence

We conducted a convergence study by refining the Lagrangian mesh of RBCs, which represent one of the critical components in our model. In the baseline case, each RBC membrane is discretized using $N_v = 642$ vertices. For the refined case, the number of vertices was increased to $N_v =$ 2562 vertices. The results, as shown in Fig. S2, compare the velocity of CTC over time for both mesh resolutions. The two curves exhibit very similar trends, indicating that the numerical solution is not significantly affected by further mesh refinement. This suggests that the original discretization is sufficiently fine to ensure the numerical accuracy and stability.

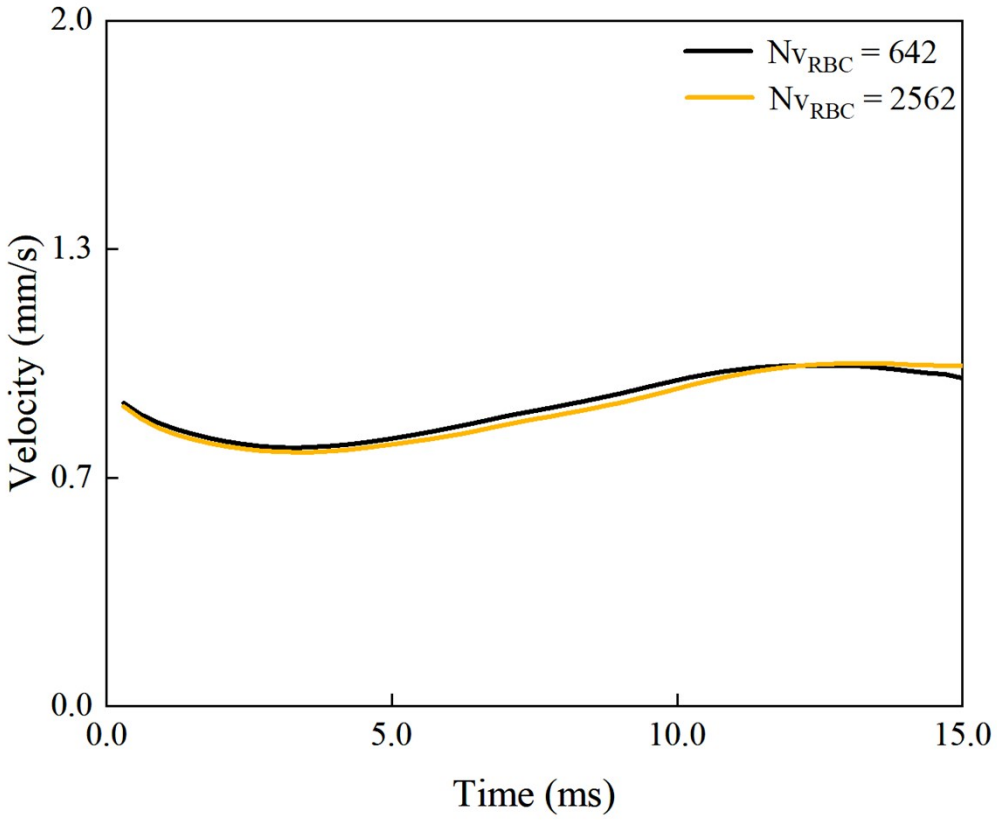

Fig. S2. CTC velocity over time

To investigate the impact of simulation time on the predictions, we extended the simulation by an additional 4.5 million timesteps under the conditions of a hematocrit of 10% and a Reynolds number of 0.01, to ensure that the final outcome would remain unchanged over time. It was observed that the firm adhesion between CTC and vessel wall, as well as the position of CTC, remained stable. Moreover, the aspect ratio of CTC increased by less than 10%. These findings indicate that the final result of the model is stable and insensitive to the simulation time span.

Cell membrane viscoelasticity and cytoplasmic viscosity

The viscoelasticity of cell membrane and the viscosity contrast between intracellular and extracellular fluids play a significant role in the cell dynamics under strong confinement. In this study, RBCs are modeled using the spectrin-link-based elastic membrane model implemented in the

HemoCell platform, which has been extensively validated for capturing large deformations and reproducing both tank-treading and tumbling behaviors. The different cell motion modes in HemoCell have been validated against the experimental data. De Haan et al. [S5] performed the Wheeler test and compared it with the experimental values, showing that the deformation index of RBCs in Couette shear flow (with shear rates between 10 and 200) is consistent with the experimental results. Závodszky et al. [S6] compared the stretching curve of the cellular material model in HemoCell with the experimental results, validating that the cellular constitutive membrane model can accurately reproduce the stretching behavior of a single RBC. Additionally, the parachute motion behavior of RBCs was also validated.

The present model does not yet account for the viscoelasticity of RBC membrane or the internal viscosity of cell. Incorporating the viscoelastic factors into the model may influence the shear force distribution exerted by RBCs on CTCs, thereby altering the quantitative characteristics such as the velocity of CTCs. Taking the increase in intracellular viscosity as an example, we performed one additional simulation, it can be observed that considering a viscosity ratio between the interior and exterior of RBCs—where the internal viscosity is five times that of the surrounding plasma—leads to a noticeable difference in CTC velocity, as shown in Fig. S3, although the overall trend remains consistent. We believe that introducing viscoelasticity will not change the main conclusions of this study, but it may introduce errors at the quantitative level. Given the significant workload required to implement and validate a viscoelastic model, we plan to further explore this topic in future research.

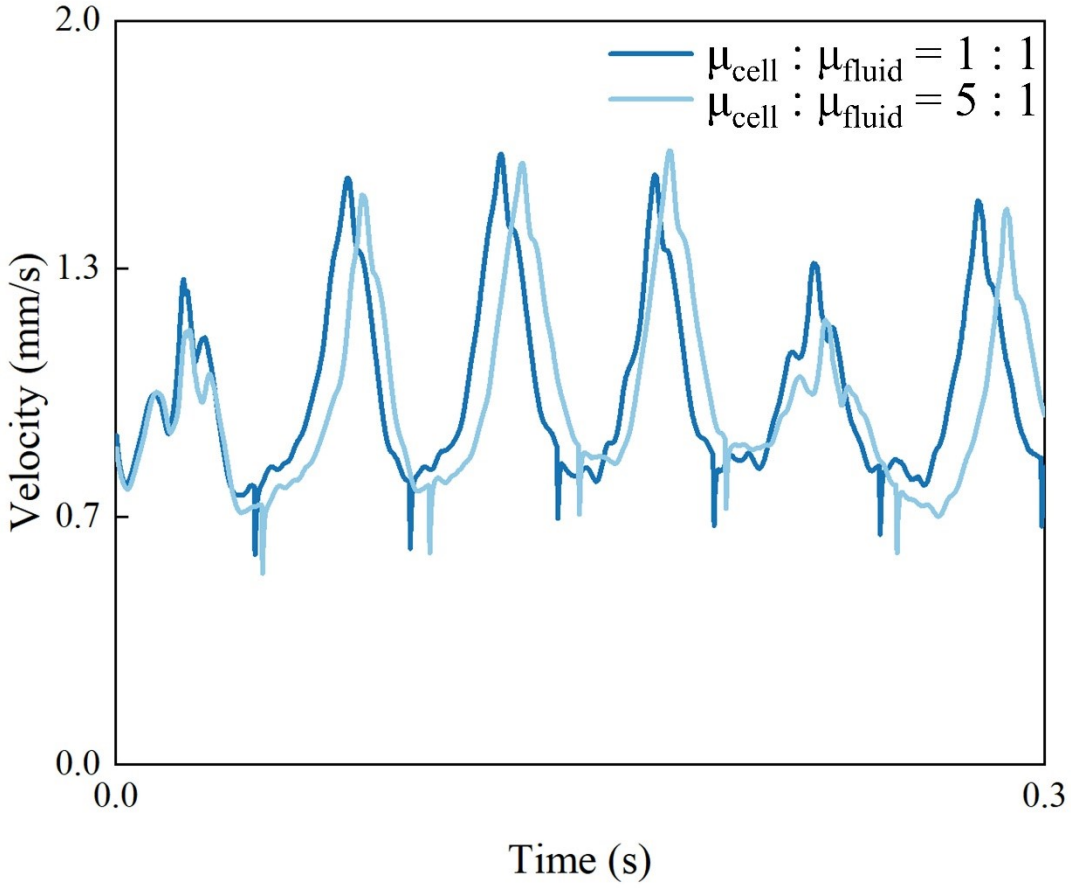

Fig. S3. CTC velocity over time at different intra-/extracellular viscosities

References

S1 G. Závodszky, B. Van Rooij, V. Azizi and A. Hoekstra, *Front. Physiol.*, 2017, **8**, 563.

S2 D. A. Fedosov, B. Caswell and G. E. Karniadakis, *Comput. Methods Appl. Mech. Eng.*, 2010, **199**, 1937–1948.

S3 W.W. Wang, T.G. Diacovo, J.C. Chen, J.B. Freund, M.R. King, *PLoS One*, 2013, **8**, e76949.

S4 H. Ye, Z. Shen, M. Wei, Y. Li, *Soft Matter*, 2021, **17**, 40-56.

S5 M. De Haan, G. Zavodszky, V. Azizi and A. G. Hoekstra, *Appl. Sci.*, 2018, **8**, 1616.

S6 G. Závodszky, B. Van Rooij, V. Azizi and A. Hoekstra, *Front. Physiol.*, 2017, **8**, 563.